Proceedings of the Seventh International Conference on Creationism.
Pittsburgh, PA: Creation Science Fellowship

EXPLAINING THE CONTINENTAL FOSSIL-BEARING SEDIMENT RECORD IN TERMS OF THE GENESIS FLOOD: INSIGHTS FROM NUMERICAL MODELING OF EROSION, SEDIMENT TRANSPORT, AND DEPOSITION PROCESSES ON A GLOBAL SCALE

John Baumgardner, Ph.D., Logos Research Associates, 24515 Novato Place, Ramona, CA 92065

KEYWORDS: turbulent sediment transport, turbulent boundary layer, open channel flow, cavitation erosion, shallow water approximation, super tide, fossil-bearing sediment record, global flood

ABSTRACT

This paper summarizes a beginning attempt to develop a numerical simulation tool for the primary erosion, transport, and sedimentation processes that operated during the Genesis Flood. It is based upon a code developed in the 1990's that solves the shallow water equations on the surface of a rotating sphere. The shallow water approximation, appropriate for this application, treats the water on the face of the earth in terms of a single vertical layer but with variable bottom height. The model assumes that the dominant means for sediment transport during the Flood was by turbulent, rapidly flowing water. Theory for open-channel turbulent flow is applied to treat the suspension, transport, and deposition of sediment. Cavitation is assumed to be the dominant process responsible for degradation of bedrock as well as for erosion of already deposited sediment. As an initial working hypothesis, horizontal accelerations required to achieve water velocities of 100-250 m/s arise from a sequence of large tides produced by repeated near approaches of a moon-sized body with the earth. An illustrative calculation shows that with plausible parameter choices a single tide 2500 m in height produces a blanket of sediment some 150 m thick on average over the continental surface in the span of only a few days. Based on this result, it is proposed that six near encounters with a moon-sized body temporarily captured by the earth can plausibly account for the six mega-sequences that are so prominent in the Phanerozoic sediment record. In particular, such large impulsive tides conceivably might explain the global erosional unconformities that define the mega-sequence boundaries.

INTRODUCTION

Accounting for the thick fossil-bearing sediment sequences that blanket the surfaces of the continents is an important issue for understanding the physical aspects of the Genesis Flood. In continental platform regions, such as the heartland of the U.S., the sequence of fossil-bearing sediments are commonly 2000 m or more in thickness (Prothero and Schwab, 2004). They also typically display astonishing horizontal continuity (e.g., Ager, 1973). Just what sort of physical

processes could have moved such huge volumes of sediment and arranged it in such orderly, laterally extensive layers within the span of a single year, as Scripture indicates? As a preliminary exercise one can make rough estimates of sorts of erosion, sediment transport, and deposition rates that are required. If we assume that most of the primary deposition occurred within the interval of 150 days during which "the water prevailed on the earth" (Genesis 7:24), we can compute an average deposition rate over that interval needed to produce a column of sediment, say, 2000 m thick. Dividing 2000 m by 150 days yields a time-averaged rate of deposition of 1.54×10^{-4} m/s or 0.56 m/hr. It also suggests a comparable rate of erosion in many places.

The large lateral extent of most of the layers suggests significant transport distances. Let us assume that the average distance between the sites of erosion and deposition is 2000 km (2×10^6 m) and that the average speed of the water is 20 m/s (45 mph). A typical sediment particle is therefore in suspension for (2×10^6 m)/(20 m/s) = 1×10^5 s (27.8 hr). If the input and output of the pipeline, so to speak, is the erosion/deposition rate of 1.54×10^{-4} m/s, then the average suspended sediment load distributed vertically through the sheet of flowing water must be (1.54×10^{-4} m/s) x (1×10^5 s) = 15.4 m. This requires that the depth of the flowing water be great enough and also its turbulence intense enough to carry this sort of suspended load. From these simple estimates it is obvious that any viable candidate mechanism likely involves coherent sheets of turbulent water at least tens of meters high sweeping over the land surface at velocities of at least tens of m/s. Since these are time-averaged estimates, when the likelihood of significant time variation, even episodicity, is taken into account, the peak water depths and speeds would likely have been substantially higher.

What might have caused water to move with such vigor across the continent surfaces? The only viable candidate mechanism I have thus far been able to identify is the tide caused by a near approach of a moon-sized or larger body. Bolide impacts, to be sure, generate tsunamis, but, guided by the crater sizes found in the geological record (Osinski, 2006), the corresponding tsunami amplitudes appear to be too feeble (Mader, 2004, pp. 233-245, "Asteroid Generated Tsunamis"). Therefore, as a working hypothesis, I assume it is the tide raised by the near approach of a moon-sized body that provides the forcing for the water motions and the resulting erosion, sediment transport and deposition processes which are modeled and described in this paper.

WHAT IS FLUID TURBULENCE?

The importance of the role of turbulence in fluids was clearly recognized in the early part of the 19th century when the pressure drop in water pipes and the drag of water on ships were hydraulics issues of considerable practical concern. It was known that both the pressure drop in pipes and the drag exerted on ships as they moved through the water had two components, one linear and the other approximately quadratic in the fluid velocity. Surprisingly it was found that only the first one depended on the viscosity of the fluid. In the 1850's G. Hagen and H. Darcy both published careful measurements of fluid flow through large pipes. They both noted that the quadratic component was associated with disordered motion in the fluid and that it became the dominant contribution when the pipes were large and the flow speed became sufficiently high.

They speculated that the increased drag was due to the energy spent in creating velocity fluctuations as the flow became turbulent.

G. Stokes (1851) was the first to show that the onset of turbulent flow depends on the ratio of the inertial force of the moving fluid to the viscous forces acting upon it. This ratio is today known as the Reynolds number, named after O. Reynolds, who in the 1870's and 1880's published a series of papers describing results of his careful experimental studies on the transition from laminar to turbulent fluid flow, first in pipes and then in other settings. Reynolds, in an 1883 paper, (Reynolds, 1883) stressed the importance of this dimensionless ratio that now bears his name. This ratio, the Reynolds number *Re*, is usually expressed as $Re = vL/\nu$, where v is the fluid velocity, L is a characteristic spatial dimension of the flow, and ν is the kinematic viscosity.

In the early 20^{th} century Ludwig Prandtl made an important computational advance by introducing the concept of a fluid boundary layer. In a groundbreaking 1905 paper he showed that the equations for fluid flow could be simplified by dividing the flow field into two regions: a boundary layer in which fluid viscosity plays a major role and (2) the region outside the boundary layer, where viscosity can be neglected with no significant effects on the solution. Prandtl's boundary layer theory provided crucial new understanding of skin friction drag and how streamlining reduces drag on airplane wings and other bodies that move relative to a fluid environment.

But what is fluid turbulence? The British scientist L. F. Richardson (1920) described fluid turbulence in poetic fashion as follows:

Big whorls have little whorls
That feed on their velocity,
And little whorls have lesser whorls
And so on to viscosity.

Richardson's picture of turbulence is a flow comprised a hierarchy of vortices, or eddies, from large to tiny. These eddies, including the large ones, are unstable. The shear that their rotation exerts on the surrounding fluid generates smaller new eddies. The kinetic energy of the large eddies is thereby passed to the smaller eddies that arise from them. These smaller eddies in turn undergo the same process, giving rise to even smaller eddies that inherit the energy of their predecessors, and so on. In this way, the energy is passed down from the large scales of motion to smaller and smaller scales until reaching a length scale sufficiently small that the molecular viscosity of the fluid transforms the kinetic energy of these tiniest eddies into heat.

In 1941, the Russian A. N. Kolmogorov postulated that for very high Reynolds numbers, the small scale turbulent motions are statistically isotropic (i.e., have no preferential spatial direction). In general, the largest scales of a flow are not isotropic, since they are determined by the particular geometrical features of the boundaries. Kolmogorov's idea was that, in the energy cascade which Richardson described, this geometrical and directional information is lost. This means that the statistics of the smaller scales has a universal character and that they are *the same for all turbulent flows* when the Reynolds number is sufficiently high. He further hypothesized that for very high Reynolds numbers the statistics of small scales are universally and uniquely

determined by the viscosity ν and the rate of energy dissipation ε. With only these two parameters, a unique length λ can be obtained by dimensional analysis given by $\lambda = (\nu^3/\varepsilon)^{1/4}$. This is today known as the Kolmogorov length scale.

Kolmogorov's concept was that turbulent flow is characterized by a hierarchy of scales through which the energy cascade takes place. Dissipation of kinetic energy occurs at scales of the order of Kolmogorov length λ, while the input of energy into the cascade comes from the decay of the large scales, characterized by scale length L. These two scales at the extremes of the cascade can differ by several orders of magnitude at high Reynolds numbers. In between there is a range of scales (each one with its own characteristic length r) that has formed at the expense of the energy of the large ones. These scales are very large compared with the Kolmogorov length, but still very small compared with the large scale of the flow (i.e., $\lambda << r << L$). Since eddies in this range are much larger than the dissipative eddies that exist at Kolmogorov scales, hardly any kinetic energy is dissipated in this range. Rather, it is merely transferred to smaller scales until viscous effects begin to become important as the Kolmogorov scale is approached. Within this range inertial effects of the moving fluid parcels are still much larger than viscous effects. Therefore within this inertial range it is possible to neglect the effects of molecular viscosity in the internal dynamics. Although some further details have emerged in the 70 years since Kolmogorov published these ideas, modern understanding of turbulence rests squarely on the basic picture he provided.

TURBULENCE IN OPEN CHANNEL FLOW

In this paper, the concern is with large-scale erosion and sediment transport and deposition processes over a continental surface driven by a rapidly moving water layer. This problem is in the general category of open channel flow, which is one of great practical interest and one that has been studied experimentally for many years. Examples of open channel flows include rivers, tidal currents, irrigation canals, and sheets of water running across the ground surface after a rain. The equations commonly used to model such flows are anchored in experimental measurements and decades of validation in many diverse applications. These experiments show that, except for the immediate vicinity of the boundary, the mean velocity profile in the turbulent flow regime is very close to being a logarithmic function of distance from the boundary. If in addition the boundary is rough due to the presence of, say, discrete sand-sized particles forming the boundary, the mean velocity $\bar{u}$ (that is, the total velocity with the high frequency fluctuations due to turbulence subtracted away) as a function of height z above the boundary is given to good approximation by

$$\bar{u}(z) = 2.5\, u_\tau \ln(z/z_o)\,, \qquad (1)$$

where u_τ is what is commonly referred to as the shear velocity or friction velocity and z_o is a number proportional to the size of the roughness elements along the boundary. This result and the brief account of turbulent boundary layer theory which follows are based on lecture notes for a 2009 graduate course entitled "Turbulent Boundary Layers" by David Apsley (2009) at the University of Manchester, UK. Apsley, in turn, relies somewhat on Pope (2000).

The quantity u_τ, defined as $u_\tau = (\tau_o/\rho)^{1/2}$, where τ_o is the boundary shear stress and ρ is the fluid density, should consciously be understood as a measure of the boundary shear stress rather than an actual velocity, even though it has dimensions of velocity and it is commonly referred to as

such. Using (1) the friction velocity u_τ can be computed from the depth h of the turbulent layer and the mean velocity at $z = h$ as $u_\tau = \bar{u}(h)/[2.5\ ln(h/z_o)]$. Assuming that the boundary roughness arises from fairly well sorted mineral sediment particles with the usual natural range of particle shape and roundness, the quantity z_o is given by $D/30$, where D is the characteristic particle size. For purposes of this paper, D is chosen to be 0.5 millimeters, the value commonly used to distinguish coarse from medium sand. The factor 2.5 is the reciprocal of the von Karman parameter, an experimentally determined quantity, named after Theodore von Kármán, a Hungarian-American aeronautical engineer considered by many to be the preeminent theoretical aerodynamicist of the 20th century.

Equation (1) provides a realistic, experimentally validated description of the mean horizontal velocity and the associated turbulence from just a few millimeters above the boundary to the top of the flowing layer. Note that the kinematic viscosity ν does not appear. This is because at the surface the drag on the surface is dominated by the roughness of the sediment particles and the turbulence this generates, rather than shearing of the water itself. The representation of the turbulent flow of equation (1) is used to connect the global water velocity field obtained by solving the shallow water equations on a rotating sphere (the earth) with the more localized model of erosion, sediment transport, and sediment deposition described below.

SUSPENDED SEDIMENT PROFILE

The following treatment of suspended sediment follows closely that provided by Harris (2003) in his lecture notes for a graduate course on sediment transport processes. Suspension of sediment particles occurs when the turbulent velocity fluctuation w' in the vertical direction is at least as large as the settling speed w of the particles. Experiments show that the vertical velocity fluctuation w' due to turbulence is approximately equal to the friction velocity u_τ, that is, $w' \approx u_\tau$ near the bottom of the turbulent layer. A quantity known as the Rouse parameter P, involving the ratio of w to u_τ and defined as $P = w/\kappa u_\tau = 2.5w/u_\tau$, is commonly used as a criterion for suspension. (κ is the von Karman parameter, whose value is 0.4) Based on experimental observation it is found that for $P > 2.5$ there is no suspension, for $1 < P < 2.5$ there is incipient suspension, and for $P < 1$ there is full suspension. Note that the particle settling speed w, and hence also the Rouse parameter P, depends on particle size.

To characterize the sediment load of the turbulent layer of water, it is useful to use the local volume fraction c of sediment in the flow. If the flow is reasonably uniform in the horizontal direction on spatial scales on the order of the layer thickness, which we shall assume, and is reasonably steady on time scales on the order of our numerical time step, then from mass conservation it can be shown that

$$\partial/\partial z[c\ w + \langle c'\ w' \rangle] = 0\ , \qquad (2)$$

where prime (‘) denotes the fluctuating component and < > denotes time average. The term $\langle c'\ w' \rangle$ represents vertical diffusion of suspended sediment by turbulent eddies. This term can be rewritten in terms of an eddy diffusivity K_s as $\langle c'\ w' \rangle = K_s\, \partial c\ /\partial z$, and equation (2) can then be rewritten as

$$\partial/\partial z[-wc - K_s \partial c/\partial z] = 0 . \quad (3)$$

Integrating this equation with respect to z yields

$$-w\,c = K_s \partial c/\partial z . \quad (4)$$

This states that for steady, uniform conditions the downward settling of sediment ($-w\,c$) balances the upward diffusion of sediment by turbulent eddies. Integrating once more with respect to height using y as the variable of integration yields

$$ln[c(z)/c(a)] = -w \int_a^z \frac{dy}{K_s(y)} , \quad (5)$$

where a is a reference height near the bed where the concentration $c(a)$ can be specified. In turbulent flow near the bed the eddy viscosity K_m for momentum is given by $K_m = \kappa u_\tau z$, where κ is the von Karman parameter, u_τ is the friction velocity, and z is height. Since the same eddies that diffuse momentum vertically also diffuse mass, one can represent the eddy diffusivity K_s as $K_s = \alpha\kappa u_\tau z$, where α is a constant of proportionality. For low sediment concentrations $\alpha \approx 1$, and for high concentrations a value of 1.35 is commonly used. Substituting this expression for K_s into the right hand side of (5) we find

$$-w \int_a^z \frac{dy}{\alpha\kappa u_\tau y} = -[w/(\alpha\kappa u_\tau)]\ ln(z/a). \quad (6)$$

Combining (5) and (6) and using the fact that the Rouse parameter $P = w/\kappa u_\tau$, we obtain the following expression for the volume fraction c of sediment as a function of height z above the bed

$$c(z)/c(a) = (z/a)^{-P/\alpha} . \quad (7)$$

This result is valid only near the base of the turbulent layer. To obtain a description that is applicable throughout the turbulent layer it is necessary to use an eddy diffusivity that decreases more strongly with height. One such functional form commonly used yields an eddy diffusivity profile that is parabolic, decreasing to zero at the top of the turbulent layer at $z = h$ and approaching $\alpha\kappa u_\tau z$ near the base of the layer. It is expressed as $K_s = \alpha\kappa u_\tau z(1 - z/h)$. Substitution of this quadratic eddy diffusivity into equation (5) yields what is known as the Rouse profile,

$$c_i(z)/c_i(a) = \{[z(h - a)]/[a(h - z)]\}^{-Pi/\alpha} . \quad (8)$$

Since the Rouse parameter depends on particle settling velocity which in turn depends on particle size, we divide the sediment into a finite number of sediment classes according to particle size which we designate by the subscript i. Equation (8) then provides a separate vertical distribution of volume fraction for each sediment class.

CARRYING CAPACITY OF THE TURBULENT FLOW

If, for the moment, we assign a value to $c_i(a)$ of unity and integrate (8) with respect to height from a to h, noting that $\{[z(h - a)]/[a(h - z)]\}^{-Pi/\alpha} = [(h/z - 1)]/[(h/a - 1)]^{Pi/\alpha}$, we obtain the following expression for the carrying capacity F_i of the flow for each sediment class

$$F_i = 1/(h/a - 1)^{P_i/\alpha} \int_a^h (h/z - 1)^{P_i/\alpha} dz \ . \qquad (9)$$

Note that F_i depends only on the Rouse parameter P_i, of the sediment class and the depth of the turbulent layer h. We choose the reference height a to be constant with a value of 1 cm. Also note that F_i, with units of distance, is the total thickness of sediment that the flow can suspend, assuming the volume fraction could reach unity at $z = a$. For practical reasons, we actually divide the height coordinate z into a number of discrete zones or layers, indexed by k, and compute a sediment carrying capacity F_i^k for each layer. The total column carrying capacity F_i is then given by $F_i = \Sigma F_i^k$, where the summation is over k. In the illustrative case we describe later, we use a total of seven vertical layers of fixed thickness to resolve the sediment profile in the turbulent flow.

SETTLING SPEED OF SEDIMENT PARTICLES

As we have seen, the ability of a turbulent flow to suspend sediment particles and maintain them in suspension depends on the settling velocity w of the particles. The Rouse parameter P that occurs as the exponent in the vertical sediment distribution formula (8) involves the ratio of the settling velocity w to the friction velocity u_τ of the turbulent flow. A great deal of experimental effort has been invested to characterize the settling velocity of sediment particles over the past 60 years. To obtain appropriate values for w we utilize a simple formula developed by Jiménez and Madsen (2003) that provides a good fit to the experimental measurements for grain sizes between 0.063 mm and 1 mm, covering the range from very fine to coarse sand. This formula is

$$w(d) = Y/(A + B/S), \qquad (10)$$

with $Y = [(s - 1) g d]^{1/2}$ and $S = 0.25 d Y/\nu$, where d is the nominal grain diameter, s is the specific gravity of the sediment grains, g is gravitational acceleration, ν is the kinematic viscosity of water, and A and B are constants arising from the fit to the data. We assume a specific gravity s for sand of 2.65, the value for g to be 9.8 m/s, and a kinematic viscosity ν for water of 10^{-6} m^2/s. The values for the constants A and B provided by Jiménez and Madsen (2003) are $A = 0.954$ and $B = 5.12$. For each sediment class i with mean nominal grain diameter d_i we apply (10) to obtain the settling velocity w_i for that sediment class. For the case described in this paper we choose three sediment classes with nominal grain diameters d_i of 0.063 mm, 0.25 mm, and 1 mm, corresponding to fine sand, medium sand, and coarse sand, respectively. Clay and silt is assumed to flocculate to form particles that display settling behavior identical to that of fine sand.

EROSION AND DEPOSITION

If the turbulent flow has not reached its capacity to suspend and transport sediment and if the flow is sufficiently rapid to erode the base, we allow for erosion and suspension of the resulting eroded particles. At present the erosion model is very simple. Since our interest is capturing the

most salient aspects of the global Flood cataclysm in which water velocities reach several tens of meters per second, we neglect erosion processes at low water velocities and instead focus on cavitation-driven erosion which occurs at higher water velocities and results in extreme erosion rates. Cavitation involves the formation of water vapor and air bubbles which occurs when local fluid pressure drops below the vapor pressure of dissolved air (Arndt, 1981). Cavitation damage arises when these bubbles are carried into regions of higher pressure and implode in the vicinity of the water-rock interface. The pressure spikes generated by the implosion and collapse of these bubbles are typically on the order of several hundred MPa, or several thousand atmospheres (Momber, 2003). Such pressure pulses exceed the shear strength of most silicate minerals. They therefore damage and erode the lattices of individual crystals that comprise a polycrystalline rock (Momber, 2003).

Whipple *et al*. (2000) provide the following simple expression to describe the rate $\dot{e}_c$ of surface degradation from cavitation erosion

$$\dot{e}_c = E(u - u_{cav})^q , \tag{11}$$

where E is a proportionality constant, u is the flow velocity just above the bed (assumed at height $z = a$), and u_{cav} is a cavitation threshold velocity. Experimentally determined values for the exponent q as large as 7 have been reported (Murai *et al*., 1997). Falvey (1990) assumes a value for q of 6. The cavitation threshold velocity u_{cav} depends of the flow depth, fine sediment concentration, dissolved air content, and Reynolds number. Chanson (1997) observes that on chute spillways and bottom outlets, cavitation damage can begin to occur at clear water velocities of between 12 to 15 m/s. Falvey (1990) suggests that cavitation can begin to occur in spillways at velocities as low as 10 m/s. For crystalline bedrock with no sediment in suspension we choose a value for u_{cav} of 15 m/s, a value for q of 6, and a value for E of $0.00001/(20 - 15)^6 = 6.4 \times 10^{-10}$, which implies an erosion rate of 10^{-5} m/s or 10 microns/s for a flow velocity at of 20 m/s at height $z = a$.

For our application, we need to account for the possible presence of a high concentration of sediment in the proximity of the surface. We do this by scaling E by the factor $(1 – 2C)$, where $C = \Sigma c_i(a)$ is the sum over all sediment classes of their volume fractions at a height $z = a$, with this sum restricted by the sedimentation treatment to be no larger than 0.5. This restriction implies that when the total sediment volume fraction reaches 50% at $z = a$, erosion ceases. For simplicity, we use these parameter values regardless of the flow depth and Reynolds number. When the bed material is sediment and not crystalline bedrock, we use the same parameters except that we increase E by a factor of five to account for the relative softness of the sediment. A test is made to ensure that all the existing sediment cover is eroded before any bedrock erosion occurs. We assume that cavitation degrades bedrock into a distribution of particle sizes corresponding to 70% fine sand, 20% medium sand, and 10% coarse sand.

We require sediment deposition to occur when the total sediment volume fraction C exceeds the value 0.5. This test is performed in the time stepping process after the new time level water velocities have been computed and the volume fraction profiles c_i for each of the sediment classes have been updated to account for the transport from the water motions during the previous time step. At that point we integrate each of the volume fraction profiles with respect to height z over the entire column to obtain thickness T_i in meters of suspended sediment in the

column. Next we apply (9) to compute the new time carrying capacity F_i of the turbulent flow based on the new time height h and new time friction velocity u_τ required in the Rouse parameter P_i. We then test to see if the sum $\Sigma T_i/F_i$ over i exceeds 0.5 or not. If the sum does not exceed 0.5, we allow erosion to occur as described above, but only the amount of erosion needed to bring the sum to the 0.5 value. On the other hand, if the sum exceeds 0.5, then sediment is removed from suspension and deposits on the bed such that the resulting sum $\Sigma T_i/F_i$ is reduced to the value 0.5. Deposited sediment is subtracted from the suspended by sediment class according to the fractional amount of sediment in the class relative to the total amount in all classes in the layer nearest the surface. Typically, the thickness of this bottom layer is chosen to be about one meter. In terms of the total suspended sediment in the column, this weighting by the relative sediment concentrations near the base of the column tends to favor deposition of coarser sediment, as should be the case, since proportionally less coarse sediment gets lofted to the upper reaches of the turbulent layer.

Following these adjustments to the class column sediment loads T_i to account for possible deposition or erosion, we compute the new time vertical sediment distribution for each sediment class consistent with equation (8). The cumulative amount of erosion and deposition as a function of position over the surface is tracked as the time stepping proceeds.

EFFECT OF SEDIMENT LOAD ON TOPOGRAPHY

It was found early in the testing the model that sediment thicknesses of several hundreds of meters routinely arise. When such large thicknesses were allowed to augment the original continent topography with no isostatic compensation whatsoever, a type of seemingly unstable behavior resulted. This behavior involved the formation of localized islands of sediment, typically a few thousand kilometers across and hundreds of meters high. This topography, in turn, forced the water flow to become concentrated in channels between these islands of sediment and for enhanced deposition to occur on top of the adjacent islands where the flow depths and velocities were small. The higher the islands grew, the stronger this tendency became. A simple remedy for this apparent pathology was to include some degree of compensation to allow the basement to subside in response to the sediment load above it. The compensation scheme chosen provides 10% compensation for loads less than 100 m, compensation increasing to 50% for a load of 500 m, and a 90% compensation for the portion of load in excess of 500 m. Symmetrical compensation is implemented for the negative loads produced by material removed by bedrock erosion.

Such nearly instantaneous compensation was found to suppress the unexpected behavior in an effective manner. However, the behavior may well not be pathological but rather may actually be reflecting physical reality. As such, it clearly merits further study. This is especially so given that the process yields more vigorous localized water flow, more intense erosion, and greater volumes of sediment. However, such further investigation will be deferred until later and is considered beyond the scope of this present paper.

COMPUTING THE TIME-DEPENDENT WATER FLOW

To model the water flow over the earth we utilize the so-called shallow water equations applied to a rotating sphere. By shallow water it is understood that the water depth is everywhere small compared to the horizontal dimensions of interest. The ocean basins on today's earth have mean

depths of about four kilometers while, by contrast, our computation grid for the earth's surface has grid point spacing of 100 km or more. The expected water depths over the continental regions where our main interest lies are yet smaller than those in the ocean basins. Therefore the shallow water approximation is an appropriate one for this problem, one that allows the water flow over the surface of the globe to be treated in terms of a single layer of water with laterally varying thickness. What otherwise would be an expensive three-dimensional problem now becomes a much more tractable two-dimensional one.

The shallow water equations on a rotating sphere may be expressed (Williamson *et al*., 1992, p. 213)

$$dh/dt \;=\; -\,h\,\nabla\cdot\mathbf{u} \tag{12}$$

and

$$d\mathbf{u}/dt \;=\; -\,f\,\mathbf{k}\times\mathbf{u} \;-\; g\,\nabla h^{\dagger}\,, \tag{13}$$

where h is water depth, $\mathbf{u}$ is horizontal velocity (on the sphere), f is the Coriolis parameter (equal to $2\Omega \sin\theta$ for rotation rate Ω and latitude θ), $\mathbf{k}$ is the outward radial unit vector, g is gravitational acceleration, and $h^{\dagger}$ is the height of the free surface above some spherical reference surface. Here it is assumed that the water is homogeneous in composition, incompressible, and invicid. If h_t denotes topography on the sphere, then $h^{\dagger} = h + h_t$. The d/dt operator is the material or substantial or co-moving time rate of change of an individual parcel of fluid. The ∇ operator is the spherical horizontal gradient operator and the $\nabla\cdot$ operator is the spherical horizontal divergence operator. Symbols in bold font correspond to vector quantities. Equation (12) is an expression of the conservation of mass, while equation (13) is an expression of the conservation of linear momentum. As mentioned above, this two-dimensional formulation in terms of a single layer in the radial direction is appropriate when the water depth is small in comparison to the important horizontal length scales.

In our problem the water depths above the continental regions are much smaller compared to those in the oceanic regions, and in these continental regions where the water is shallow we expect strong turbulence. Therefore, the assumption that the flow is invicid is not an appropriate one, and we need to account for the strong drag that occurs at the continent-water interface. A simple means for doing this is to add a bottom friction term on the right hand side of equation (13) of the form $-\beta\mathbf{u}/(h+1)$, where β is a scaling parameter with units of m/s. Because the terms in equation (13) have dimensions of force per unit mass, this drag term requires the division by water depth h to be consistent. The addition of 1 to h in the denominator is to prevent the overall term from becoming excessively large as the water depth approaches zero. It is also common in ocean models to include in the momentum equation a so-called eddy viscosity term that seeks to represent the effects of turbulence on scales not resolved by the computational grid. The simplest such formulation is a term proportional to the 2-D Laplacian operator $\nabla^2 = \nabla\cdot\nabla$ on the sphere applied to the velocity field, that is, a term of the form $\gamma\,\nabla^2\mathbf{u}$, where γ is a scaling parameter with units m^2/s. Note that γ depends on the grid resolution. Typical values are $1\text{x}10^{-3}$ for β and $2\text{x}10^{-11}$ for γ when the grid spacing is 120 km. Adding these two terms to the right hand side of the momentum equation (13) yields

$$d\mathbf{u}/dt \;=\; -\,f\,\mathbf{k}\times\mathbf{u} \;-\; g\,\nabla h^{\dagger} - \beta\mathbf{u}/(h+1) + \gamma\nabla^2\mathbf{u}\,, \tag{14}$$

Note that in continental regions the water depth can decrease to zero. We therefore constrain the water depth h always to be non-negative and the water velocity u to be zero when h is zero. We also constrain the right hand side of equation (14) to be zero when h is zero.

These equations are solved in discrete fashion on a mesh constructed from the regular icosahedron as shown in Fig. 1. The mesh has 40962 nodes and the spacing between nodes is about 120 km. A separate spherical coordinate system is defined at each node such that the equator of the system passes through the node and the local longitude and latitude axes are aligned with the global east and north directions. This approach has the advantage that the coordinates are almost Cartesian and only two (tangential) velocity components are needed. A semi-Lagrangian formulation (Staniforth and Cote, 1991) of equations (12) and (14) is used which involves computing the trajectories during the time step that end at each node. Values for h and $\boldsymbol{u}$ at the beginning of the time step at the starting point of each trajectory are found by interpolating from the known nodal values at the beginning of the time step. Changes in h and $\boldsymbol{u}$ along the trajectory are computed using (12) and (14). This Lagrangian-like method eliminates most of the numerical diffusion that is associated with Eulerian schemes. Second-order accurate interpolation is used to find the starting point values of the trajectories. This formulation using the icosahedral mesh has been carefully validated using the suite of test problems developed by Williamson *et al*. (1992). It also forms the basis for the global weather forecast model known as GME developed in the late 1990's by the German Weather Service which in now used by more than 20 other nations (Majewski, *et al.*, 2002).

HORIZONTAL ACCELERATIONS DRIVING THE WATER FLOW

The large lateral extent that characterizes a significant fraction of the continental Paleozoic and Mesozoic sediment layers appears almost certainly to require forcing acting coherently over large spatial scales. What are the candidate mechanisms that could accelerate the water covering much of the earth in a manner that would cause sheets of water, coherent on large spatial scales, to sweep over the continent regions at speeds of many tens of m/s? One possibility I considered was the torque and accompanying angular accelerations exerted by a planetary body if it passed close to the earth. Upon running the numbers, however, I concluded that such effects would be small compared with those associated with the tide that a close planetary encounter also would generate. The gravitational potential W of the tide caused by the close encounter of a body of mass m that comes within a distance R from the center of the earth is given by (Stacey, 1977, p.92)

$$W = G\frac{ma^2}{R^3}\left(\frac{3}{2}\cos^2\psi - \frac{1}{2}\right), \tag{15}$$

where G is the universal gravitational constant, a is the earth's radius, and ψ is the angle between a given point on the earth's surface and the line connecting the center of the earth and the center of the passing body. The height h_{td} of the tide is given by $h_{td} = W/g$, where g is the gravitational acceleration at the earth's surface. Given that $g = Gm_e/a^2$, where m_e is the earth's mass, we can express the tidal height as

$$h_{td}(\psi) = \frac{ma^4}{m_e R^3}\left(\frac{3}{2}\cos^2\psi - \frac{1}{2}\right). \tag{16}$$

The tidal height is maximum when $\psi = 0$. For a specified maximum tidal height h_{max}, we observe that

$$R = \left[\frac{ma}{m_e h_{max}}\right]^{1/3} a \qquad (17)$$

Note that from (16) the tidal minimum is $-0.5h_{max}$.

AN ILLUSTRATIVE CASE

To illustrate the global sediment patterns this treatment produces we choose a simple geometry of a single circular continent, centered at the equator and zero degrees longitude, covering 38% of the earth's surface. The oceanic region surrounding the continent is taken to have a uniform height of -4000 m relative to the mean sea level. The height of the continent at its center is 150 m relative to mean sea level and smoothly decreases to -24 m at its edge. Initially the water is at rest with its surface at sea level. The continent surface is assumed everywhere to consist of crystalline bedrock. At the beginning of the calculation, it is assumed that a body with a mass at least 0.3% of that of the earth makes a near approach across a point at (90°E, 30°N) so as to raise a 2500 m high tide at that location and also 180° away on the opposite side of the earth. If the body has a mass exactly 1% of that of the earth, from (17) the distance R at closest approach is $2.94a$, or 18,740 km from the earth's center. This distance is comfortably beyond the Roche limit. The earth's gravity acting on the tidal displacements generates water flow with speeds exceeding 270 m/s. We note that by comparison the moon's mass is 0.0123 times that of the earth.

Sediment generated from the resulting bedrock erosion is suspended in the turbulent water that quickly spreads across the continent surface. Wherever the suspended sediment load exceeds the carrying capacity of the turbulent flow, sediment deposition occurs. Once a sediment layer is present, it is vulnerable to being eroded, suspended, and transported before being re-deposited elsewhere. Bedrock erosion and sediment deposition generate topographical relief on the continent surface, relief that also affects the pattern of water flow. These highly dynamical processes continue until friction between the moving water and the earth's surface dissipates the gravitational potential energy of the tide and the water speeds become too small to drive the strongly erosive turbulent water flow any longer.

Figures 2-5 provides four snapshots, spaced 12 hours apart, from the beginning of the calculation showing respectively (i) the instantaneous thickness of sediment suspended by the turbulent flow, (ii) the net amount of sediment remaining on the surface as a result of the ongoing processes of deposition and erosion, (iii) the cumulative bedrock erosion, and (iv) the topography of the continental surface as erosion and deposition and isostatic compensation jointly act to alter it. Peak water speeds over this two-day interval range from about 270 m/s down to 100 m/s, far beyond the cavitation onset value of 15 m/s. The turbulent surges of water that sweep across the continent during this interval are of sufficient depth and speed to suspend more than 100 meters of sediment in certain regions and to transport it for thousands of kilometers. However, drag from the stationary continent surface on the moving water dissipates its kinetic energy, especially when it begins to become shallow. Rapid deposition then occurs under those conditions. The four snapshots of Figure 3 show how dynamic these processes are and how rapidly sediment can deposit and accumulate. In this illustrative case most of the erosion occurs along the margin of

the continent where surges from the ocean basin impinge upon the continent. Given the strength of the turbulent flow, this sediment is efficiently transported far into the continent interior. Erosion and deposition also alter the topography, which in turn affects the flow and the flow's sediment carrying capacity.

Figure 6 provides a more detailed picture of the suspended and deposited sediment separated into the three assumed sediment classes. As mentioned earlier we assume that the erosional processes, especially cavitation, reduce crystalline bedrock into a mixture of relatively fine particles, 70% with a mean diameter of 0.063 mm corresponding to that of fine sand, 20% with a mean diameter of 0.25 mm corresponding to medium sand, and 10% with a mean diameter of 1 mm corresponding to coarse sand. Figure 6 displays the lateral distribution of suspended sediment for each size class at a time of 1 day. It also shows the lateral distribution of the deposited sediment by size class at this same time. Coarse particles have a much higher settling velocity than fine particles and hence are more difficult to suspend and also are the first to fall from suspension as the flow velocity decreases. These coarse particles therefore tend to be deposited closer to their source.

The suspended sediment distribution, net cumulative deposited sediment distribution, cumulative erosion distribution, and continent topography at a time of 5 days are displayed in Figure 7. A significant fraction of the continental area is now blanketed with sediment, including some regions which earlier had experienced large amounts of bedrock erosion. The total cumulative amount of erosion is sufficient to cover the continent with sediment to an average depth of 157 m. The peak velocity of the water flow is now 92 m/s, and the average thickness of suspended sediment is 4.8 m.

DISCUSSION

The main purpose of this paper is to describe this initial attempt to realize a numerical model for the primary erosion, sediment transport, and deposition processes that operated during the Genesis Flood to generate today's fossil-bearing sediment record. A key aspect of the model is the application of the equations for open channel turbulent flow developed and utilized widely in the hydraulic engineering and marine science communities. The range of validity of these equations appears to include the regime of higher velocities and water depths expected in a continent-scale flood. However, it is important to recognize that these equations describe only a subset of the spectrum of transport, deposition, and erosion mechanisms that occurred during the Flood. The open channel flow equations, for example, do not capture the physics of submarine mud flows and debris flows. Nonetheless, it is my personal conviction that a majority of the sediment erosion, transport, and deposition during the Flood must have involved rapidly flowing turbulent water. In other words, while transport by turbulent water certainly does not account for all aspects of the Flood sediment record, in my assessment it likely must represent the dominant transport mechanism.

Another key aspect of the model described in this paper is the reliance on cavitation for the high rates of erosion implied by the Flood record. While application of the equations describing open channel turbulent flow to the scale of the global Flood seems eminently justifiable, limitations in the observations as well as in the theory that undergird the current understanding of cavitation processes suggest the need for much more caution when extrapolating cavitation to conditions that may have prevailed during the Flood. Most of the relevant observations and experiments

concern cavitation damage to concrete spillway structures of large dams (e.g., Falvey, 1990; Chanson, 1997). The discovery that cavitation can be usefully applied to rock drilling has prompted laboratory studies relating to these applications (e.g., Momber, 2003), so more experimental data for the regime of extremely high water velocities and associated cavitation rates may be forthcoming.

In regard to the role of cavitation in natural bedrock erosion, the literature is meager. Whipple *et al.* (2000) include cavitation along with plucking, abrasion, and solution in their analysis of fluvial bedrock erosion processes. While they acknowledge in their abstract that "new analysis indicates that cavitation is more likely to occur in natural systems than previously argued", nevertheless they add that "direct field evidence for cavitation erosion, however, is lacking." In any case, we do utilize their equation (13), which is our equation (11), for the rate equation we apply for cavitation erosion. We note, however, that the authors express caution and add the qualification, "despite a vast and rapidly growing literature, at present we are unable to provide a more robust scaling of cavitation wear."

The most crucial term in (11) is the exponent q, which several authors put in the range of 5-7. This means that the cavitation erosion rate is extremely sensitive to the water speed u once it exceeds the cavitation threshold u_{cav}. For example, with q equal to 6, doubling the difference between u and u_{cav} increases the cavitation erosion rate by a factor of 64. The range for q between 5 and 7 does seem to be based on reliable observations. On the other hand, the multiplicative factor E in (11) is not that well constrained by experimental data. Falvey (1990, p. 34) mentions an experiment in which a 13 mm hole was produced in concrete over a period of 3 hours by a 30 m/s jet, but almost no details of the experiment are provided. These numbers suggest an erosion rate of 1.2×10^{-6} m/s. However, in the context of mentioning the experiment Falvey cautions the reader, "Presently, correlations have not been developed that quantify the amount of damage, of a given material, for a specified amount of cavitation." More recently Momber (2003) reports experimental work to measure relative rates of cavitation erosion for various types of rocks and concrete using a cavitation chamber. Crucial details of the experiment are not included in the paper. Nevertheless, using erosion rates provided in mg/s and estimating the area of damage from the photographs in the paper, one infers erosion rates for granite and rhyolite on the order of 4×10^{-5} m/s. The point here is that there is a moderate level of uncertainty in the value assumed for the parameter E (10^{-5} m/s for a water speed of 20 m/s) in the cavitation portion of the model.

One of the most important issues that emerges from the illustrative calculation is that the average depth of sediment, about 150 m, eroded from and deposited upon the continent represents only a small fraction of Phanerozoic sediment we actually observe on the continents today. Moreover, the vast majority of the erosion, transport, and deposition unfolds in less than five days' time. Although there is some leeway in the choice of the magnitude of the tide and perhaps in the value of E in the cavitation erosion rate, there does not seem to be a way to escape the conclusion that a single giant tide induced by the near approach of a moderate-sized extraterrestrial body simply cannot account for the entire fossil-bearing sediment record. The tidal amplitude is restricted by the amount of water in the oceans and also limited by a plausible maximum value on water velocity. The duration of its effects also seems to be too brief to square with the description provided in the Genesis account.

However, some important clues for possibly resolving these issues are found in the sediment record itself. A striking characteristic of the Phanerozoic continental sediment record is that it is organized into a few globally extensive, unconformity-bounded packages, known as mega-sequences. The concept of globally synchronous unconformities, presumably produced by dramatic eustatic lowering of sea level, together with the remarkable preservation of such global unconformities across a continent was introduced by Lawrence Sloss in 1963. Sloss (1963) identified six mega-sequences which he named Sauk, Tippecanoe, Kaskaskia, Absaroka, Zuni, and Tejas, draped the North American craton, as depicted in Figure 8. He also showed that craton-wide unconformities separate these massive packages of sediment from one another. It has since been verified that this pattern of six unconformity-bounded mega-sequences is indeed global in extent. Uniformitarian earth scientists have inferred that this pattern is a consequence of the rise and fall in eustatic sea level. The mechanism they generally propose to cause such global sea level variation is a fluctuation in the rate of seafloor spreading, which alters the average temperature of the ocean lithosphere and therefore the volume of the ocean basins and hence sea level. But gradual changes in eustatic sea level seem woefully inadequate to account for the craton-wide unconformities, even in a uniformitarian framework. In the context of the Genesis Flood a catastrophic explanation is obviously required.

The sort of water flow that emerges in the illustrative case described above appears to be consistent with what would be required to produce one of sedimentary mega-sequences, especially the continent-wide erosional unconformity at its base. Certainly, giant tidal surges with flow velocities exceeding 200 m/s represent staggering erosive power, power sufficient even to reduce mountain belts to smooth surfaces. These numerical results therefore seem able to account for one of the most astonishing features of the sedimentary record, namely, the craton-wide smooth unconformity surfaces separating the mega-sequences. In addition, the general pattern of sediment fining upward through each mega-sequence, that is, generally progressing from sand, to silt, to clay, is precisely what should be expected as the water masses lose their kinetic energy and the eroded particles settle out of suspension.

I therefore cautiously propose a scenario of multiple close approaches by the same body in a highly eccentric orbit, with each close approach raising a tide on the order of 2500 m high. Based on the prominence of six mega-sequences in the Phanerozoic record, I explored the possibility that there might have been exactly six close approaches. To be able to raise a tide on the order of 2500 m and also to remain beyond the Roche limit at closest approach, the mass of body must exceed about a fourth the mass of the moon. Of course, the smaller the mass of the body, the easier it is for the earth temporarily to capture it. If the body made only six close approaches with the earth, then presumably an interaction with some other body caused it subsequently to break free of the earth's gravitational dominance.

What might the time interval have been between the tidal pulses? Rather arbitrarily I chose an interval of seven days, such that six tidal pulses fit within the first 40 days of the Flood cataclysm. I assumed that the geometry of the orbit of the body as well as its phase relative to the rotating earth were identical for all six tidal pulses. Figure 9 shows snapshots of the total suspended sediment, the net cumulative deposited sediment, the cumulative bedrock erosion, and the topography at a time of 30 days after the onset of the first pulse. This snapshot is at two days

after the onset of the fifth tidal pulse. At a time of five days after the sixth pulse and 40 days after the onset of the first pulse, the average amount of sediment blanketing the continent is 680 m. In this simple scenario, the first pulse generates an average of 157 m of sediment, and subsequent pulses add about 100 m each. This comes within about a factor of two of the amount of Phanerozoic sediment we actually observe.

Without debate, this is a speculative scenario. Nevertheless, the mega-sequences, so prominent in the sediment record, particularly the global erosional unconformities that divide one mega-sequence from the next, are features that cry out for explanation. I therefore meekly offer this scenario as a candidate attempt to account for these observations.

SUMMARY AND CONCLUSION

This paper presents a beginning attempt to model numerically the primary erosion, transport, and sedimentation processes that occurred during the Genesis Flood to account for a large fraction of the continental fossil-bearing sediment record. It utilizes standard theory for open channel turbulent flow in the suspension, transport and deposition of sediment. It assumes that cavitation is the primary agent responsible for bedrock as well as sediment erosion and uses the standard scaling for cavitation erosion rate as a function of water speed. The model treats the water on the earth's surface in terms of a single layer of water with variable bottom topography, an approximation known as the shallow water approximation. It uses a computational grid consisting of almost equal area triangles covering the spherical surface. It utilizes a semi-Lagrangian scheme, a scheme with very little numerical diffusion, for horizontal transport of momentum, water, and sediment. As a place-holder in this study, water motion is driven by a large tide raised by the near approach of a planet-sized body coincident with the onset of the Flood. The gravitational potential energy associated with this tide is dissipated by friction between the moving water and the solid earth beneath, mostly in continental regions where the water depths are small.

A simple case, which assumes a single circular continent covering 38% of the earth, with the continent surface consisting entire of crystalline bedrock and slightly submerged by water around its perimeter, is used to illustrate how the model behaves. Although the water initially is at rest, accelerations from the giant tidal perturbation quickly lead to water velocities of 270 m/s and more, with high levels of turbulence, intense cavitation erosion, and sediment suspended and transported for thousands of kilometers, as surges of water rush into the continent interior. The flow pattern becomes more complex as sedimentation and erosion alter the originally smooth topography and surges interact with one another. These processes continue, with accumulation of an increasing volume of eroded sediment with time blanketing the continent in a complex pattern, until bottom friction dissipates most of the tidal energy. In this particular run, an average of about 150 m of sediment covers the continent after only 5 days. The average is over the entire continent, including the eroded portions. The case shows that the numerical treatments work as intended and that plausible parameter choices leave a significant blanket of sediment over much of the continental surface, most of which remains above the mean sea level. When that initial case of a single tidal pulse is extended to include five identical additional pulses spaced seven days apart, then the total sediment volume approaches what is actually observed in the Phanerozoic record.

It is to be noted that the cases described in this paper do not include any initial continental topography apart from a slightly domed surface, nor any dynamic topography arising from tectonic or volcanic/magmatic processes apart from modest isostatic adjustment from erosion and sediment load, nor any easily eroded sediment initially present on the continental surface, nor any dynamic changes in the depth of the ocean basin, nor any changes to the spatial distribution of the continental blocks, nor any motions of the deposited sediments due to gravity-driven debris flows, nor any effects of chemically precipitated sediment material, nor any contributions from plucking or suspended load abrasion to bedrock erosion, nor any of a much longer list of processes that undoubted affected the sediment distribution in significant ways. Moreover, there are a multitude of possibilities for the choice of direction for the fly-by of the extraterrestrial body; each yields a different time history of horizontal accelerations, some significantly so. The point here is that this numerical model is a beginning framework that can be augmented and applied to address an immense spectrum of issues relating to the Flood. Hopefully, many colleagues, especially younger ones, will apply it to specific topics they have a passion and calling to explore.

REFERENCES

Ager, D.V. (1973). *The nature of the stratigraphical record*. London: MacMillan, 114 p.

Apsley, D.D. (2009). Structure of a turbulent boundary layer (lecture notes from course entitled 'Turbulent Boundary Layers", spring semester, 2009, at Manchester University, UK). Posted at http://personalpages.manchester.ac.uk/staff/david.d.apsley/lectures/turbbl/regions.pdf

Arndt, R.E.A. (1981). Cavitation in fluid machinery and hydraulic structures. *Annual Reviews of Fluid Mechanics, 13*, 273–328.

Chanson, H. (1997). *Air Bubble Entrainment in Free-Surface Turbulent Shear Flows*. London: Academic Press, 401 p.; http://staff.civil.uq.edu.au/h.chanson/aer_dev.html#References.

Darcy, H. (1857). Recherches expérimentales relatives au mouvement de l'eau dans les tuyaux (Experimental research relative to the movement of water in pipes). Paris: Mallet-Bachelier.

Falvey, H.T. (1990). *Cavitation in chutes and spillways*. Denver, CO: U. S. Bureau of Reclamation, Engineering Monograph No. 42, 160 p.

Hagen, G. (1854). Über den Einfluss der Temperatur auf die Bewegung des Wassers in Röhren (On the influence of temperature on the motion of water in pipes). *Math. Ahh. Akad. Wiss. Berlin*, 17-98.

Harris, C.K. (2003). Suspended sediment transport (lecture notes from graduate course entitled "Sediment Transport Processes in Coastal Environments" at Virginia Institute of Marine Science). Posted at http://www.vims.edu/~ckharris/MS698_03/lecture_08.pdf.

Jiménez, J. and Madsen, O. (2003). A simple formula to estimate settling velocity of natural sediments. *J. Waterway, Port, Coastal, Ocean Eng.*, 129(2), 70–78.

Kolmogorov, A.N. (1941). The local structure of turbulence in incompressible viscous fluids at very large Reynolds numbers. *Dokl. Akad. Nauk. SSSR 30*, 299-303. Reprinted in *Proc. R. Soc. London A 434*, 9-13, 1991.

Kolmogorov, A.N. (1941). Dissipation of energy in isotropic turbulence. *Dokl. Akad. Nauk. SSSR*, 32, 19-21.

Mader, C.L. (2004). *Numerical Modeling of Water Waves, 2nd ed.*, Boca Raton, FL: CRC Press.

Majewski, D., Liermann, D., Prohl, P., Ritter, B., Buchhold, M., Hanisch, T., Paul, G., Wergen, W., and Baumgardner, J. (2002). The global icosahedral-hexagonal grid point model GME: Operational version and high resolution tests. *Monthly Weather Review, 130*, 319-338.

Momber, A.W. (2003). Cavitation damage to geomaterials in a flowing system. *Journal of Materials Science, 38*, 747-757.

Murai, H., Nishi, S., Shimizu, S., Murakami,Y., Hara,Y., Kuroda, T., and Yaguchi, S. (1997). Velocity dependence of cavitation damage (sheet-type cavitation). *Transactions of the Japan Society of Mechanical Engineers, Part B, 63: 607*, 750–756.

Osinski G.R. (2006). The geological record of meteorite impacts. *1st International Conference on Impact Cratering in the Solar System*. Noordwijk, Netherlands. Posted at http://www.psi.edu/explorecraters/Osinski-ESASP06.pdf (accessed Sept. 4, 2012).

Pope, S.B. (2000). *Turbulent Flows*, Cambridge University Press, 771 p.

Prandtl, L. (1905). Uber Fleussigkeitsbewegungen bei sehr kleiner Reibung (On fluid flow with very little friction). in Verhandlungen des dritten internationalen Mathematischen Kongresses, Heidelberg, Teubner Verlag, Leipzig, 484-491.

Prothero, D.R. and Schwab, F. (2004). *Sedimentary geology: An introduction to sedimentary rocks and stratigraphy 2nd Edition*. New York: W.H. Freeman, 12-14.

Reynolds, O. (1883). An experimental investigation of the circumstances which determine whether the motion of water shall be direct or sinuous, and of the law of resistance in parallel channels. *Philosophical Transactions of the Royal Society*, *174*, 935–982.

Richardson, L.F. (1920). The supply of energy from and to atmospheric eddies. *Proceedings of the Royal Society of London, Series A, 97:686*, 354-37.

Sloss, L.L. (1963). Sequences in the cratonic interior of North America. *Geological Society of America*

Bulletin, 74, 93–113.

Stacey, F.D. (1977) *Physics of the Earth, 2nd ed.*, New York: John Wiley & Sons, 414 p.

Staniforth, A. and Cote, J. (1991). Semi-Lagrangian integration schemes for atmospheric models--a review. *Monthly Weather Review, 119,* 2206-2223.

Stokes, G. (1851). On the effect of the internal friction of fluids on the motion of pendulums, *Trans. Cambridge Phil. Soc. 9,* 8–106.

Whipple, K.X., Hancock, G.S., and Anderson, R.S. (2000). River incision into bedrock: mechanics and relative efficacy of plucking, abrasion and cavitation, *GSA Bulletin, 112,* 490-503.

Williamson, D.L., Drake, J.B. Hack, J.J., Jakob, R. and Swatztrauber, P.N. (1992). A standard test set for numerical approximations to the shallow water equations in spherical geometry, *Journal of Computational Physics, 102:1*, pp. 211-224.

FIGURES

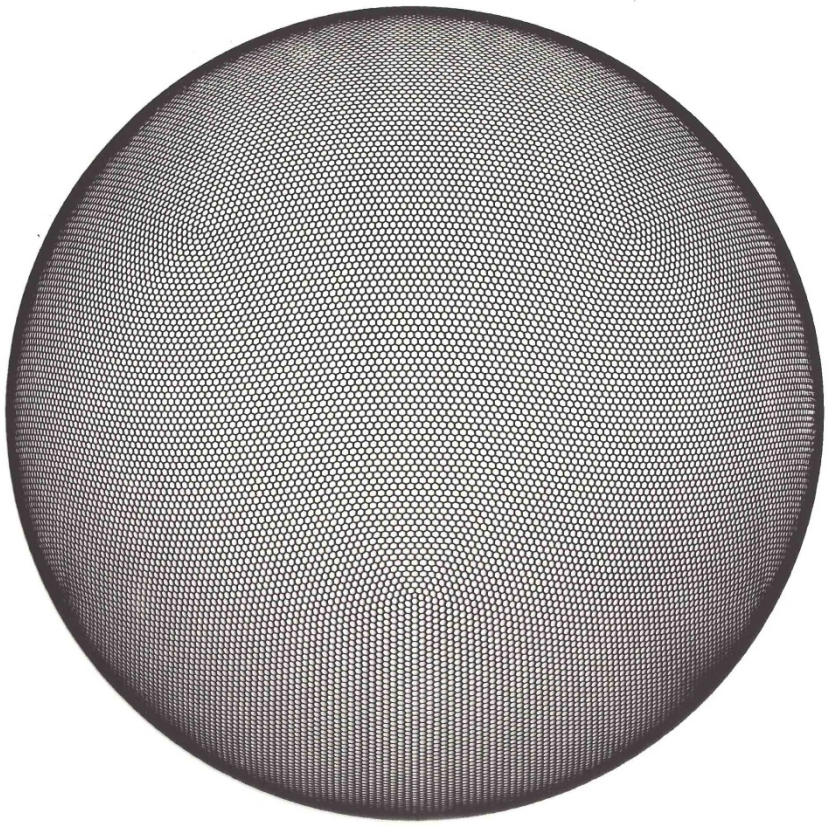

Figure 1. Computational grid used in illustrative case. Constructed from the regular icosahedron, this grid provides an almost uniform discretization of the spherical surface. It has 40962 cells with an average cell width of about 120 km for the surface of the earth.

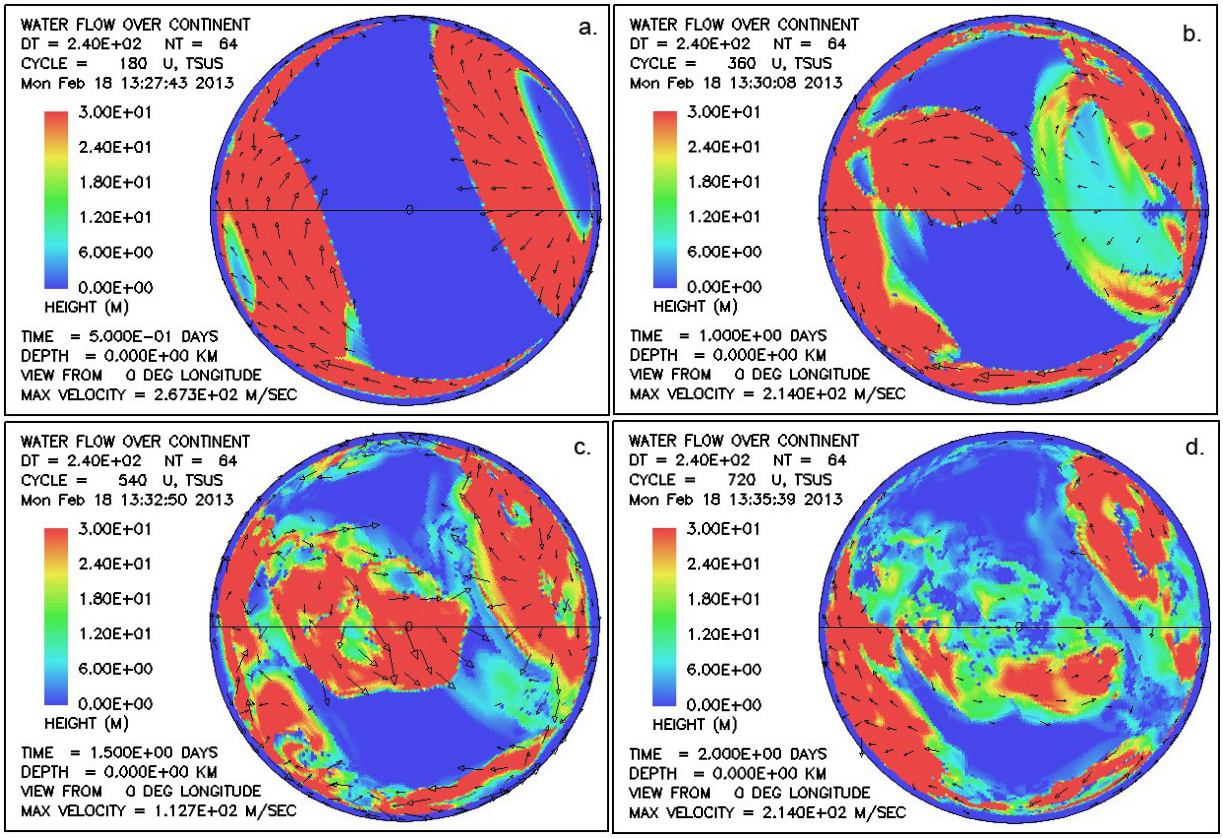

Figure 2. Snapshots from the illustrative case of the solid equivalent thickness of suspended sediment (sum over all sediment classes) at (a) 0.5 day; (b) 1 day; (c) 1.5 days; and (d) 2 days.

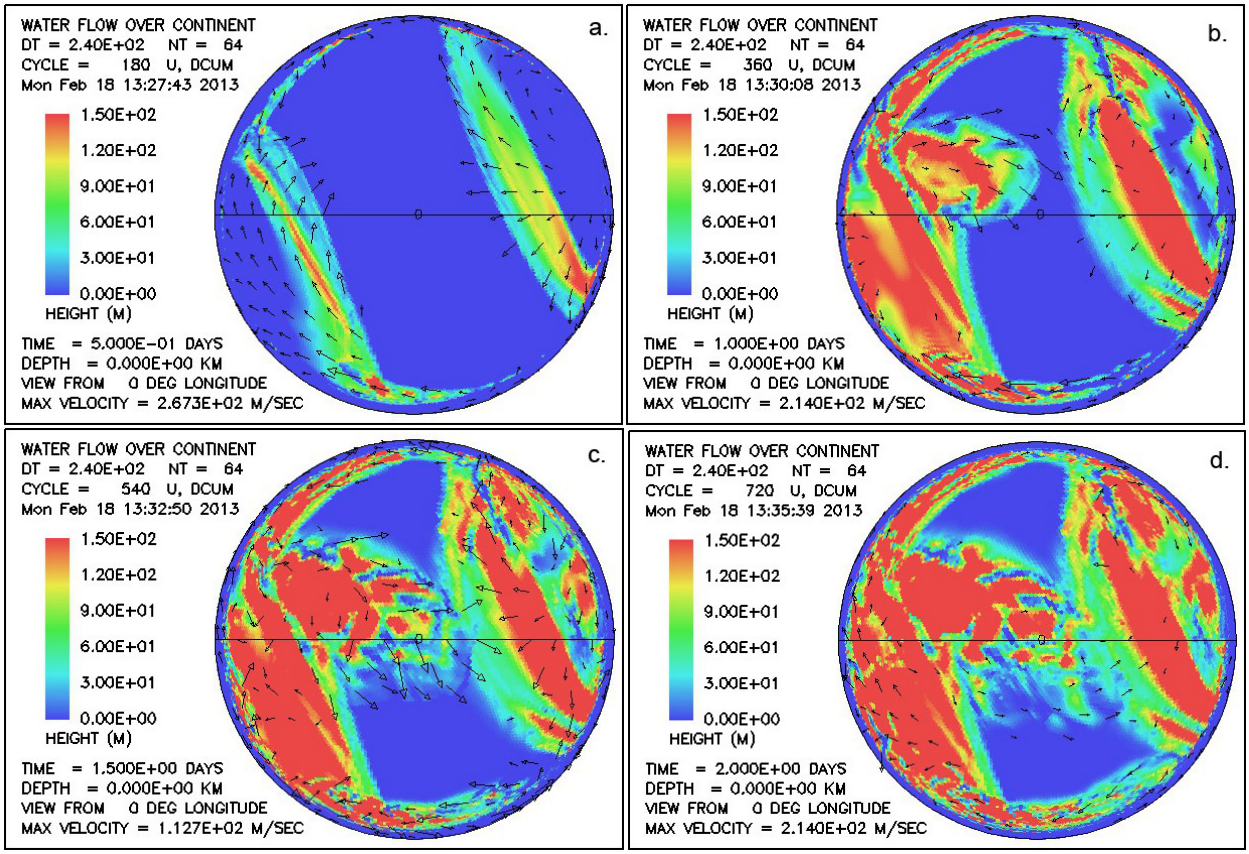

Figure 3. Snapshots from the illustrative case of the net cumulative thickness of deposited sediment (sum over all sediment classes) at (a) 0.5 day; (b) 1 day; (c) 1.5 days; and (d) 2 days.

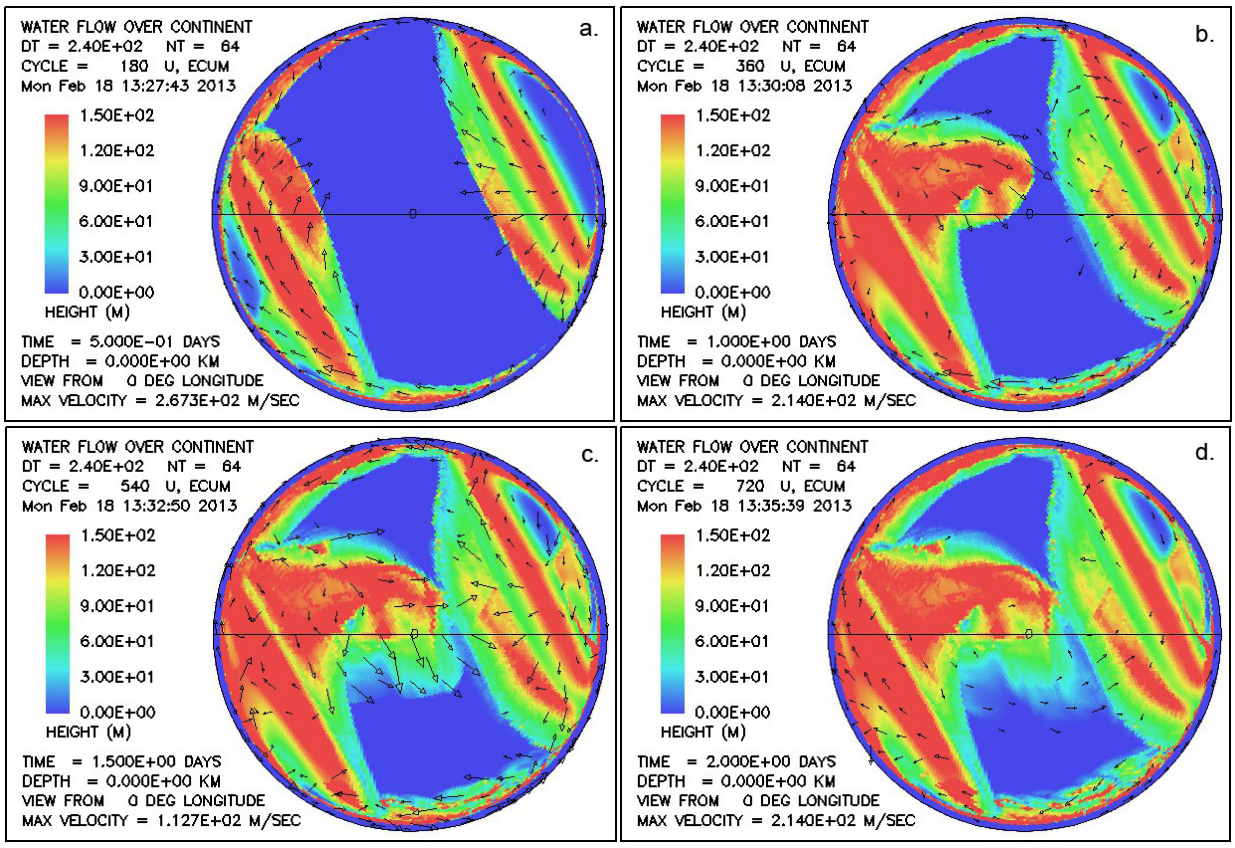

Figure 4. Snapshots from the illustrative case of the cumulative bedrock erosion at (a) 0.5 day; (b) 1 day; (c) 1.5 days; and (d) 2 days.

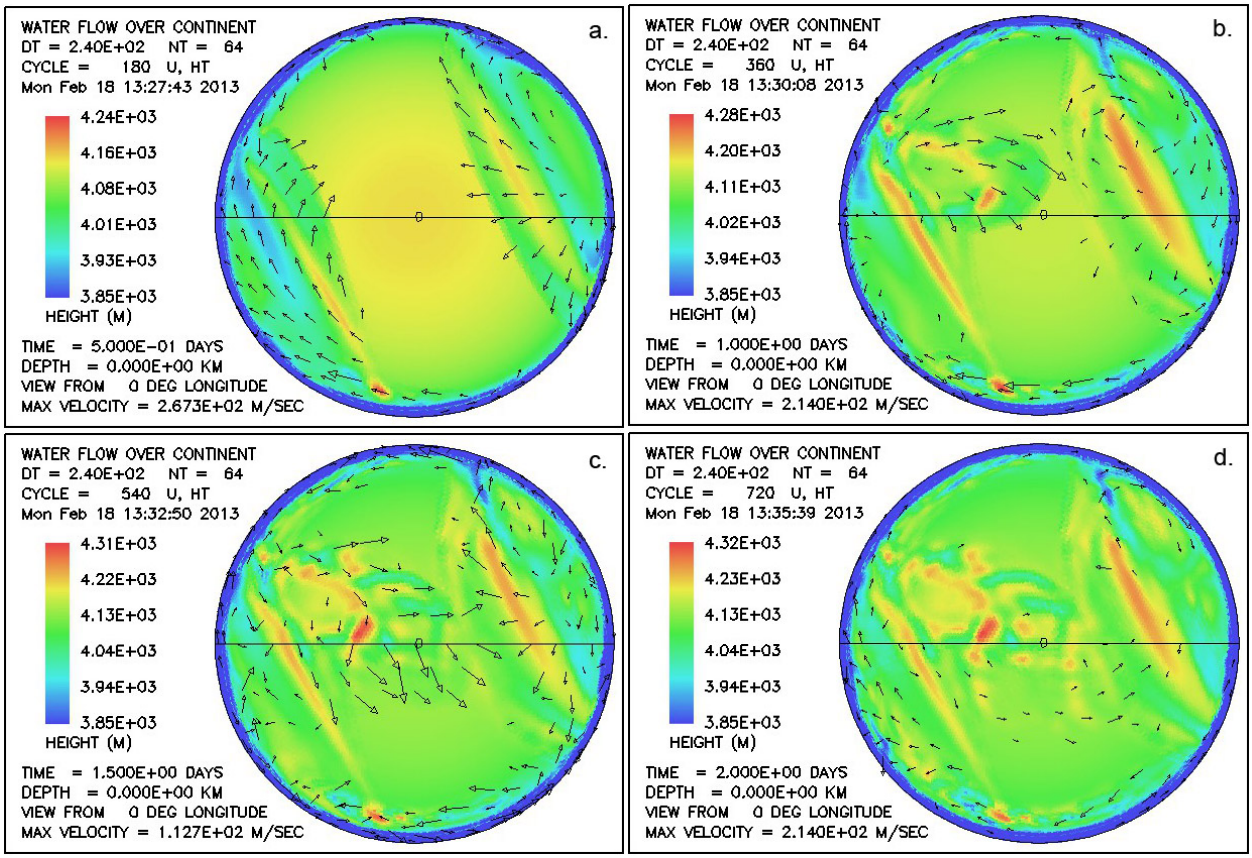

Figure 5. Snapshots from the illustrative case of the continent surface topography at (a) 0.5 day; (b) 1 day; (c) 1.5 days; and (d) 2 days. Note that the height scale changes with time.

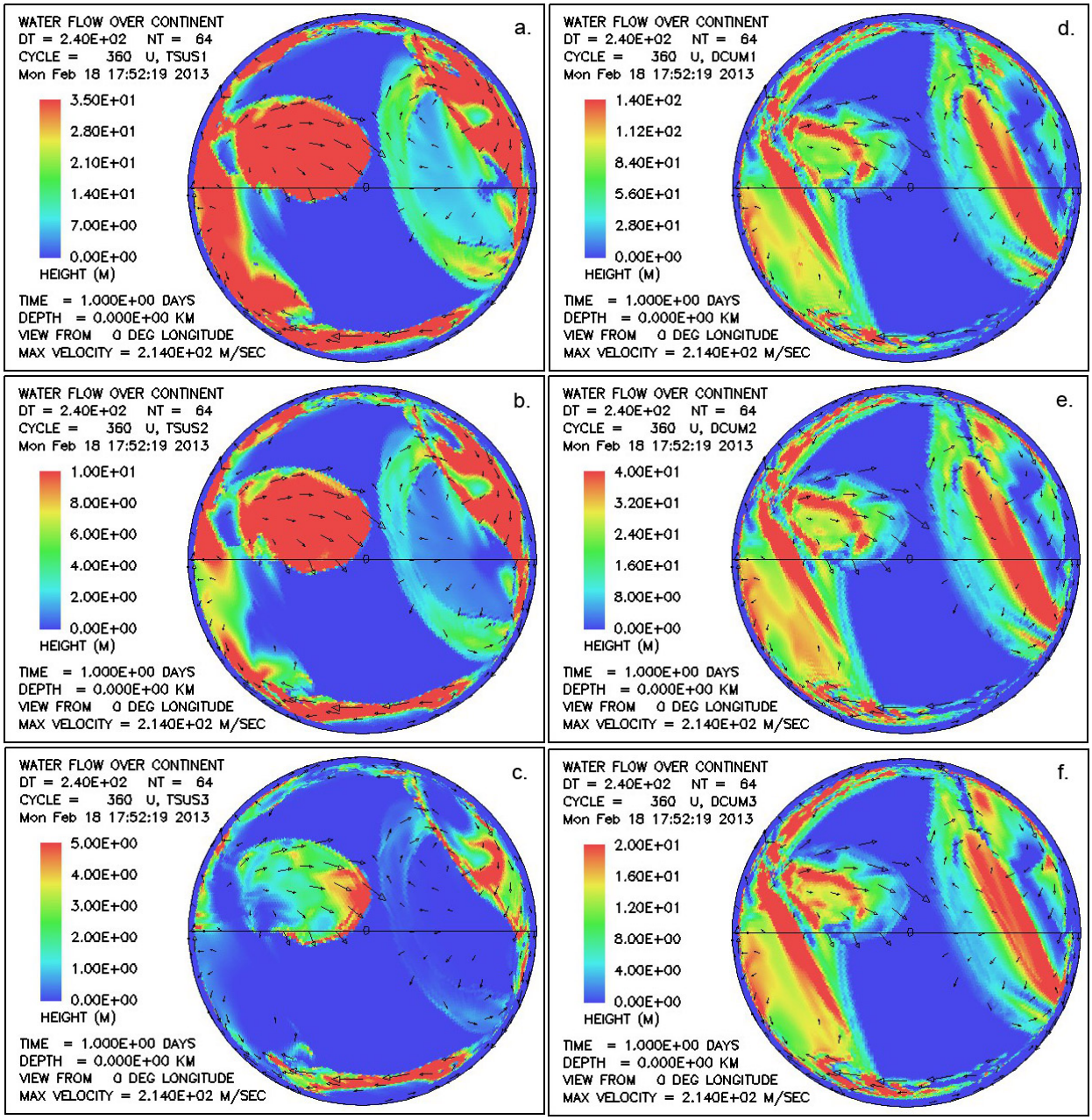

Figure 6. Snapshot at a time of 1 day from illustrative case: (a) suspended fine sand; (b) suspended medium sand; (c) suspended coarse sand; (d) cumulative deposited fine sand; (e) cumulative deposited medium sand; (f) cumulative deposited coarse sand. Amplitudes of the plots are scaled to match the 70:20:10 volume ratios for the three particle size classes produced by bedrock erosion.

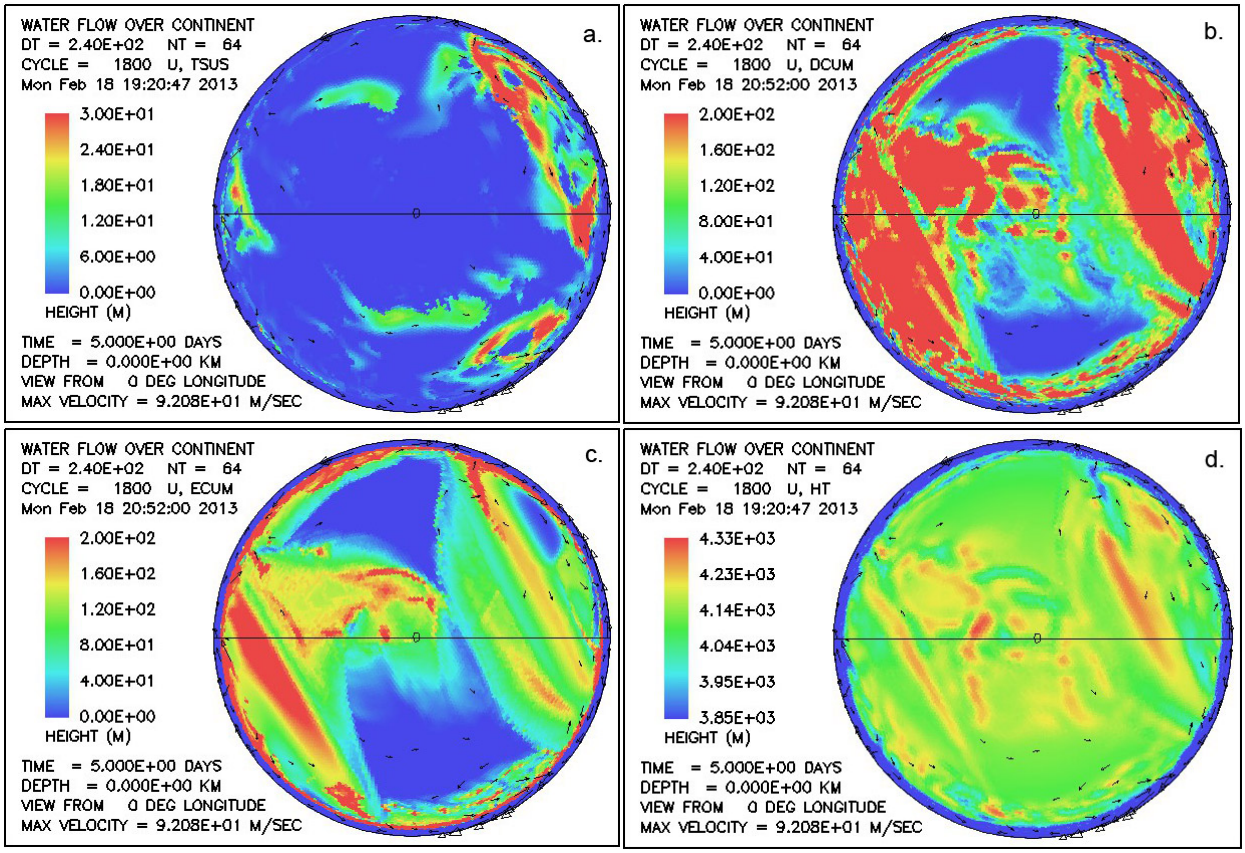

Figure 7. Snapshot at 5 days from the illustrative case: (a) suspended sediment (sum over sediment classes); (b) net cumulative deposited sediment (sum over sediment classes); (c) cumulative bedrock erosion; and (d) topography. Note that, except for the suspended sediment plot, the scale maxima differ from those of Figures 2-5.

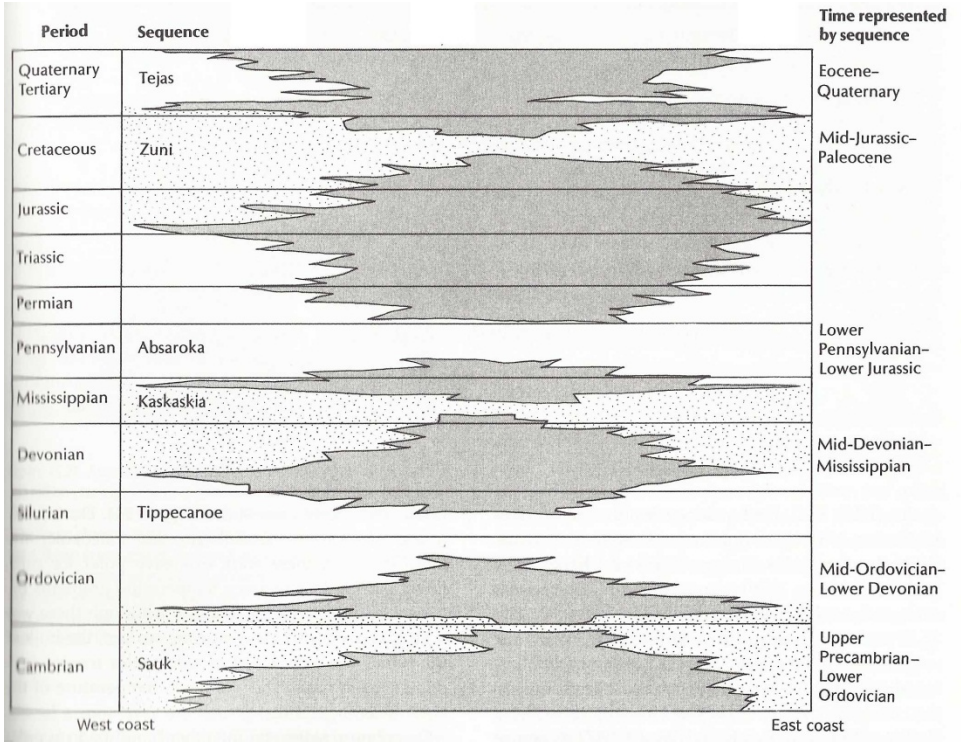

Figure 8. Sloss (1963) diagram of unconformity-bounded mega-sequences in North America. Dark areas represent gaps in the stratigraphic record, presumably due to either non-deposition or erosion. White and stippled areas represent sediment. Alternation between white and stippled is used to distinguish one mega-sequence from the next.

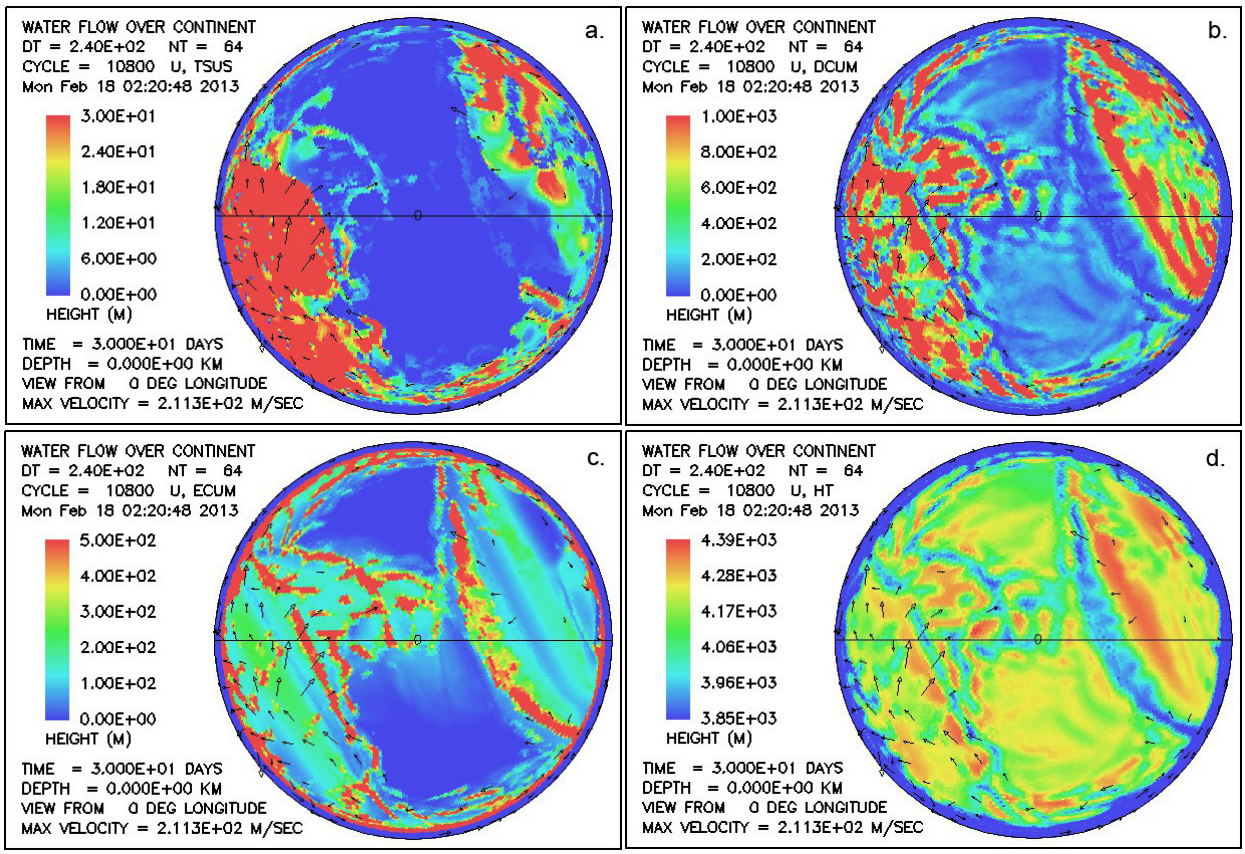

Figure 9. Snapshot at 30 days from the illustrative case: (a) suspended sediment (sum over sediment classes); (b) net cumulative deposited sediment (sum over sediment classes); (c) cumulative bedrock erosion; and (d) topography. This snapshot is at two days after the onset of the fifth tidal pulse. Note that, except for the suspended sediment plot, the scale maxima differ from those of Figures 2-5.